Int. J. Electrochem. Sci., 9 **(2014)** 4816 - 4825

International Journal of
ELECTROCHEMICAL
SCIENCE
www.electrochemsci.org

In Situ Synthesis of Nanosized $Li_4Ti_5O_{12}$/Graphene/carbon Nano-Tubes Hybrid Materials for High Rate Rechargeable Lithium Ion Batteries

Xing Li[1,2,*], *Ying Zhou*[1,2], *Pengxiao Huang*[1], *Hui Peng*[1], *Wen Li*[3], *Meizhen Qu*[3,*], *Zuolong Yu*[3], *Xiaobing Huang*[4], *Yuandao Chen*[4]

[1]School of Materials Science and Engineering, Southwest Petroleum University, Chengdu 610500, China
[2]State Key Laboratory of Oil and Gas Reservoir Geology and Exploitation, Southwest Petroleum University, Chengdu 610500, China
[3]Chengdu Institute of Organic Chemistry, Chinese Academy of Science, Chengdu 610041, China
[4]College of Chemistry and Chemical Engineering, Hunan University of Arts and Science, Changde 415000, China
[*]E-mail: lixing@swpu.edu.cn (X. Li), mzhqu@cioc.ac.cn (M.Z. Qu)

Received: 7 May 2014 / *Accepted:* 12 June 2014 / *Published:* 16 June 2014

We report a facile sol-gel approach to in situ synthesize a $Li_4Ti_5O_{12}$/graphene/carbon nano-tubes ($Li_4Ti_5O_{12}$/G/CNTs) hybrid material. The hybrid material consists of nanostructured $Li_4Ti_5O_{12}$ particles and conductive second phases (graphene and CNTs), which is favorable to improve both of the Li^+ and electronic conductivity of the spinel $Li_4Ti_5O_{12}$. The CNTs in the hybrid material play a role as bridges, which can give more effectively conductive nets in the electrode by connecting the graphene and the $Li_4Ti_5O_{12}$ particles that can not anchor on the surface of graphene. With the addition of 3 wt.% of graphene and CNTs, the $Li_4Ti_5O_{12}$/G/CNTs hybrid material exhibits excellent rate capability and cycling performance. At the charge/discharge rate of 0.5 C, its initial discharge specific capacity is 174 mA h/g, which is very close to the theoretical value of the spinel $Li_4Ti_5O_{12}$ (175 mAh/g), and even at a very high charge/discharge rate of 30.0 C, the $Li_4Ti_5O_{12}$/G/CNTs hybrid material can still deliver a discharge specific capacity of 150 mAh/g. Moreover, only less than 1% discharge capacity loss over 100 cycles at 10.0 C is observed. The outstanding electrochemical performances of the nanosized $Li_4Ti_5O_{12}$/G/CNTs hybrid material make it a promising anode material for high rate lithium ion batteries.

Keywords: lithium titanate; graphene; carbon nano-tubes; high rate anode materials; Lithium-ion batteries

1. INTRODUCTION

Spinel lithium titanate ($Li_4Ti_5O_{12}$) has been demonstrated as a highly promising anode electrode material for LIBs [1-3]. It features a higher lithium intercalation-deintercalation potential (about 1.55 V vs. Li/Li^+), which can effectively prevent safety problems associated with carbon-based anodes [4]. Furthermore, the spinel $Li_4Ti_5O_{12}$ possesses excellent structural stability and an almost negligible volume change during the Li^+ insertion and extraction processes, which suggests virtually unlimited cycle life [5]. All of these merits indicate that $Li_4Ti_5O_{12}$ is advantageous as an anode for high power LIBs with safety, long life and reliability. However, the intrinsic low electrical conductivity (ca. 10^{-13} S cm^{-1}) makes the $Li_4Ti_5O_{12}$ suffer from the problem of poor rate capability, which is unfavorable to the power density of LIBs [6]. In order to improve the rate capability of the $Li_4Ti_5O_{12}$, various approaches have been developed, which include doping $Li_4Ti_5O_{12}$ with aliovalent metal ions [7-10], synthesizing nanosized $Li_4Ti_5O_{12}$ particles [11-13], and forming a hybrid material consisting of nanosized $Li_4Ti_5O_{12}$ and a conductive second phase such as carbon [14-16], noble metal [17, 18], graphene [19-21] and carbon nanotubes (CNTs) [22]. Among the above mentioned hybrid materials, the nanosized $Li_4Ti_5O_{12}$ has higher electrode/electrolyte contact area and shorter path lengths for Li^+ transport, which is favorable to improve the Li^+ conductivity. In addition, the conductive second phase in the hybrid material can improve the surface electronic conductivity of the spinel $Li_4Ti_5O_{12}$. These indicate that the hybrid materials composed of nanostructured $Li_4Ti_5O_{12}$ and conductive second phase could be an ideal material both for rapid ionic and electronic transport, which are required for good rate capability. However, the conductive second phase in the hybrid material is usually single, and it might obtain better rate capability via synthesizing a $Li_4Ti_5O_{12}$ hybrid material consisting of two conductive second phases.

In the present study, we synthesized nanosized $Li_4Ti_5O_{12}$/graphene/carbon nano-tubes ($Li_4Ti_5O_{12}$/G/CNTs) hybrid material via a facile sol-gel reaction route. The $Li_4Ti_5O_{12}$/G/CNTs hybrid material consist of nanostructured $Li_4Ti_5O_{12}$ particles and conductive second phases (graphene and CNTs), which is favorable to improve both of the Li^+ and electronic conductivity of the spinel $Li_4Ti_5O_{12}$. Using the sol-gel method, nanostructured $Li_4Ti_5O_{12}$ can be synthesized. Furthermore, the nanosized $Li_4Ti_5O_{12}$ particles can be homogeneously anchored on the surface of the graphene. The CNTs in the hybrid material act like bridges, which could give more effective conductive nets in the electrode and make the nanosized $Li_4Ti_5O_{12}$/G/CNTs hybrid material has better rate capability.

2. EXPERIMENTAL

2.1. Material synthesis

All materials and chemicals in the present study were purchased commercially and used as received. Graphene with a diameter of 5 μm and a thickness of 4.5 nm was purchased from Chengdu Organic Chemicals Co., Ltd. The CNTs were multiwall, with a diameter and length of about 30 nm

and 2 μm respectively, which were also purchased from Chengdu Organic Chemicals Co., Ltd. Other chemical reagents were purchased from Kelong Chemical Reagents Company.

The nanosized $Li_4Ti_5O_{12}$/G/CNTs hybrid material was synthesized by a sol-gel method and the detailed procedures were introduced as following. Firstly, 8.5 ml of Tetrabutyl titanate (Ti-$(OC_4H_9)_4$) was dissolved in 60 mL of absolute ethyl alcohol to form a stable solution. Then, the graphene and CNTs using Polyvinylpyrrolidone (PVP) as dispersant were dispersed in the above solution with sufficient ultrasonication to form a uniform suspension liquid. About 0.86 g lithium hydroxide monohydrate ($LiOH \cdot H_2O$) was dissolved in another 20 mL of absolute ethyl alcohol in a beaker to form a stable solution. Subsequently, the $LiOH \cdot H_2O$ solution was transfer to the suspension liquid of Ti-$(OC_4H_9)_4$ with vigorous stirring to form a sol system. The sol system was heated at 60℃ for 24 h with circulation reflux under constant stirring to form a gel system. The gel system was then heated at 90℃ to remove solvents gradually, and became a precursor of the nanosize $Li_4Ti_5O_{12}$/G/CNTs. Finally, the precursor powder was calcinated at 800℃ for 12 h in Ar atmosphere to obtain the nanosized $Li_4Ti_5O_{12}$/G/CNTs hybrid material. The total quantity of graphene and CNTs in the hybrid was given as 3 wt.%, and the mass ratio of the graphene and CNTs in the hybrid was 1:1. The pristine nanosized $Li_4Ti_5O_{12}$ was also synthesized using a similar sol-gel reaction route as mentioned above.

2.2. Materials characterization

The X-ray diffraction (XRD) patterns of the nanosized $Li_4Ti_5O_{12}$/G/CNTs hybrid material and the pristine $Li_4Ti_5O_{12}$ were recorded using the Philips X' Pert Pro MPD DY1219 with a Cu K_α radiation source. Particle morphologies and microstructures of the samples were observed by scanning electronic microscopy (SEM FEI INSPECT-F) and transmission electron microscopy (TEM) images were recorded on a FEI Tecnai G220 microscope operated at 200 KV. The amounts of graphene and CNTs in the nanosized $Li_4Ti_5O_{12}$/G/CNTs hybrid materials were measured by thermogravimetry (TG) method with a heating rate of 10 ^{0}C in air atmosphere from 25 ^{0}C to 900 ^{0}C by HENVEN HCT-1. Specific surface areas of the samples were evaluated via nitrogen adsorption/desorption at −196 ^{0}C using a Builder SSA-4200 apparatus.

2.3. Electrochemical measurements

The electrochemical performances of the nanosized $Li_4Ti_5O_{12}$/G/CNTs hybrid material and the pristine $Li_4Ti_5O_{12}$ were measured using a two-electrode coin-type half cell (CR2032), which consists of positive electrode (working electrode), a Celgard 2400 separator, and a lithium foil as negative electrode. The working electrode was composed of 90 wt.% nanosized $Li_4Ti_5O_{12}$/G/CNTs or pristine $Li_4Ti_5O_{12}$ active material, 5 wt.% acetylene black and 5 wt.% LA-132 binder, which was prepared as follows: first, the active material, acetylene black and binder were mixed and ground to form a uniform slurry, then the slurry was coated onto an aluminum foil and dried under vacuum at 120 ^{0}C for 12 h, finally the foil was cut into disks (13 mm in diameter) as the working electrode. The active mass and electrode thickness of the working electrode are about 4.0 mg and 50 μm, respectively. The electrolyte

was 1 M $LiPF_6$/EC:DEC:DMC (1:1:1 in volume). The cells were assembled in a glove box filled with high purity argon gas. Galvanostatic discharge–charge measurements were carried out at a constant cut-off voltage of 1–3 V at room temperature (NEWARE Electronic Co. Ltd, China). Cyclic voltammograms of the samples were recorded from 1 V to 3 V with a scan rate of 0.2 mV/s using Autolab Pgstat302N electrochemical workstation, and the AC impedance spectrums were measured by using a Solatron 1260 Impedance Analyzer in the frequency range 10^{-2}–10^{6} Hz with a potential perturbation at 10 mV.

3. RESULTS AND DISCUSSION

3.1. Characterization of the pristine nanosized $Li_4Ti_5O_{12}$ and the nanosized $Li_4Ti_5O_{12}$/G/CNTs hybrid material

X-ray diffraction patterns of the samples are shown in Fig.1. It can be observed that the patterns of the pristine $Li_4Ti_5O_{12}$ and the $Li_4Ti_5O_{12}$/G/CNTs hybrid material are similar. Moreover, all peaks of the above samples can be indexed as spinel $Li_4Ti_5O_{12}$ according to JCPDS File No. 26-1198. These results indicate that the addition of graphene and CNTs in the precursor does not affect the formation of spinel $Li_4Ti_5O_{12}$ during heat-treatment process. The quantity of the added graphene and carbon nano-tubes in the hybrid material measured by TG in air atmosphere is about 3 wt.% which is equal to the quantity added in the precursor, indicating that there is almost no loss of the graphene and CNTs during the synthesis process and the structure of the graphene and CNTs is maintained [21].

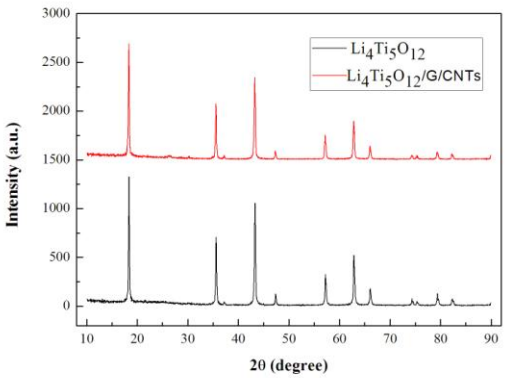

Figure 1. XRD patterns of the pristine $Li_4Ti_5O_{12}$ and the $Li_4Ti_5O_{12}$/G/CNTs hybrid material.

Fig.2 shows the SEM images of the pristine $Li_4Ti_5O_{12}$ and the $Li_4Ti_5O_{12}$/G/CNTs hybrid material. From the images of the samples, it can be seen that the primary particles of both of the samples are nanosized (less than 100 nm). However, the $Li_4Ti_5O_{12}$/G/CNTs hybrid material (Fig.2b) has less agglomeration than that of the pristine $Li_4Ti_5O_{12}$ (Fig.2a). The BET surface areas of the pristine $Li_4Ti_5O_{12}$ and the $Li_4Ti_5O_{12}$/G/CNTs are 28.4 m^2/g and 33.9 m^2/g, respectively. These results

indicate that the $Li_4Ti_5O_{12}$/G/CNTs hybrid material has bigger BET surface area in comparison with the pristine $Li_4Ti_5O_{12}$, which should be ascribed to that the addition of graphene and CNTs in the precursor could hinder the particle agglomeration and growth during the calcination process.

From the image of the $Li_4Ti_5O_{12}$/G/CNTs hybrid material (Fig.2b), it can be observed that the $Li_4Ti_5O_{12}$ can anchor on the surface of the graphene nanosheets via the sol-gel approach. In addition, the surface of the CNTs also been covered with a layer of $Li_4Ti_5O_{12}$. Fig.2b also shows that part of the bigger $Li_4Ti_5O_{12}$ particles can not anchor on the surface of the graphene. Nevertheless, the CNTs acting like bridges, which can connect the graphene and the bigger $Li_4Ti_5O_{12}$ particles, giving a more effective conductive connection between the graphene and the $Li_4Ti_5O_{12}$ in the hybrid material.

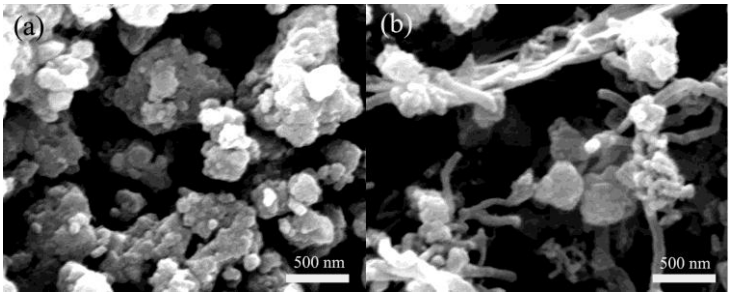

Figure 2. SEM images of the pristine $Li_4Ti_5O_{12}$ (a) and the $Li_4Ti_5O_{12}$/G/CNTs hybrid material (b).

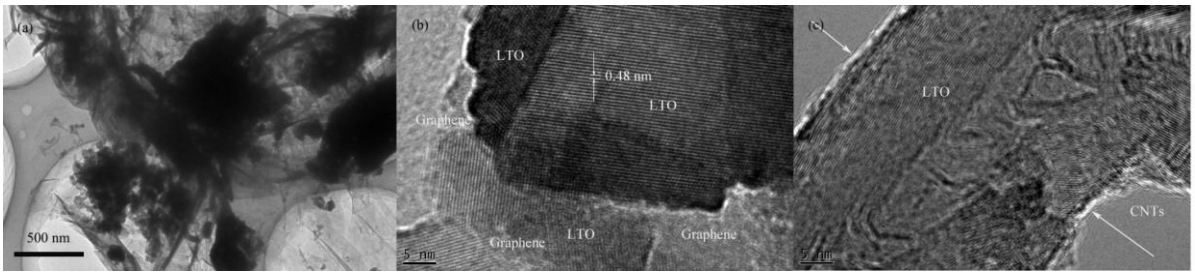

Figure 3. TEM images of the $Li_4Ti_5O_{12}$/G/CNTs hybrid material.

TEM provides further insight into the morphology and microstructure of the $Li_4Ti_5O_{12}$/G/CNTs hybrid material, as shown in Fig. 3. From image a, it can also be observed that there is a more effective conductive connection existing in the $Li_4Ti_5O_{12}$/G/CNTs hybrid material, which is obviously favorable to improve the electronic conductivity of the insulated $Li_4Ti_5O_{12}$. The contact between the graphene and $Li_4Ti_5O_{12}$, and the contact between the CNTs and $Li_4Ti_5O_{12}$ can be observed from the high resolution TEM images as shown in image b and image c, respectively. Image b shows that there is $Li_4Ti_5O_{12}$ particle anchoring on the surface of the graphene, and the $Li_4Ti_5O_{12}$ particle has a well-crystallized structure with 0.48 nm lattice spacing, which is consistent with the lattice spacing of (111) plane. Image c also shows that there is a layer of $Li_4Ti_5O_{12}$ covered on the surface of the carbon nano-tubes. These results indicates that the $Li_4Ti_5O_{12}$ can anchor or cover on the surface of the graphene and carbon nano-tubes via using a sol-gel method.

3.2. Electrochemical performance

Fig.4 shows the cyclic voltammograms (CV) of the electrodes of the $Li_4Ti_5O_{12}$/G/CNTs hybrid material and the pristine $Li_4Ti_5O_{12}$ at a scan rate of 0.2 mV/s between 1 V and 3 V. It can be observed that all the investigated electrodes have similar redox peaks between 1 V and 3 V. However, the redox peaks of the $Li_4Ti_5O_{12}$/G/CNTs are much sharper and better-resolved in comparison with the pristine $Li_4Ti_5O_{12}$. It is well known that a sharp and well-resolved peak generally signifies fast Li^+ insertion/deinsertion. The CV of the samples indicate that the $Li_4Ti_5O_{12}$/G/CNTs hybrid material has faster Li^+ conductivity than that of the pristine $Li_4Ti_5O_{12}$, which should be ascribed to that the $Li_4Ti_5O_{12}$/G/CNTs hybrid material has less particle agglomeration and bigger BET surface area than that of the pristine $Li_4Ti_5O_{12}$.

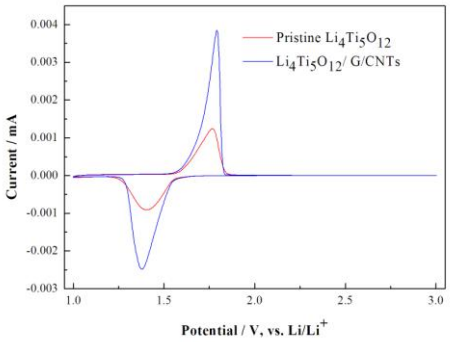

Figure 4. Cyclic voltammograms of the pristine $Li_4Ti_5O_{12}$ and the $Li_4Ti_5O_{12}$/G/CNTs hybrid material electrodes.

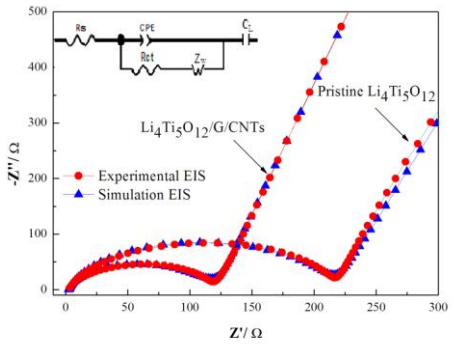

Figure 5. AC impedance spectra with the equivalent circuit of the pristine $Li_4Ti_5O_{12}$ and the $Li_4Ti_5O_{12}$/G/CNTs hybrid material electrodes.

Table 1. Impedance parameters calculated from equivalent circuits.

Materials	$R_s(\Omega)$	$R_{ct}(\Omega)$	i^o (mA/cm^2)
pristine $Li_4Ti_5O_{12}$	2.714	204.5	0.127
$Li_4Ti_5O_{12}$/G/CNTs	2.485	101.9	0.252

The AC impedance spectra of the $Li_4Ti_5O_{12}$/G/CNTs hybrid material and the pristine $Li_4Ti_5O_{12}$ are shown in Fig.5, which are measured at the stable voltage of 1.55V, respectively. As shown in Fig.5, the AC impedance spectra are simulated by Z-view software using same equivalent circuit. It can be observed that the experimental and simulated AC impedance spectra are almost coincident, which indicates that the AC impedance spectra of the $Li_4Ti_5O_{12}$/G/CNTs and $Li_4Ti_5O_{12}$ electrode all fit the equivalent circuit. According to the equivalent circuit, the AC impedance spectra of the depressed semicircle at high-middle frequency range represent the charge transfer resistance at the particle/electrolyte interface (R_{ct}). The slope line at low frequency corresponds to the Warburg impedance (Z_W). The R_s in the equivalent circuit is the resistance of the electrolyte, the constant phase element (CPE) is placed to represent the double-layer capacitance and the C_L is the insertion capacitance at the applied potential [23]. Table 1 shows the parameters of the recorded equivalent circuit, from which it can be observed that both the R_s and R_{ct} of the $Li_4Ti_5O_{12}$/G/CNTs hybrid material are smaller than that of the pristine $Li_4Ti_5O_{12}$, whereas the exchange current densities (i^0 = RT/nFRct) of the $Li_4Ti_5O_{12}$/G/CNTs is larger than the pristine $Li_4Ti_5O_{12}$. These results indicate that the $Li_4Ti_5O_{12}$/G/CNTs hybrid material has better electronic conductivity than that of the pristine $Li_4Ti_5O_{12}$, which should be attributed to that there is a more effective conductive connection within the hybrid material of $Li_4Ti_5O_{12}$/G/CNTs.

Fig.6 shows the cyclic performances of the pristine $Li_4Ti_5O_{12}$ and the $Li_4Ti_5O_{12}$/G/CNTs hybrid material at different rates from 0.5 C, 1.0 C, 3.0 C, 5.0 C, 10.0 C, 20.0 C to 30.0 C and then in returned from 30.0 C to 0.5 C between 1 V and 3 V. The charge-discharge processes of the samples are carried out for 10 cycles for different rates mentioned above, respectively. It can be observed that the pristine $Li_4Ti_5O_{12}$ sample exhibits a lower discharge specific capacity especial at high rates as compared with the $Li_4Ti_5O_{12}$/G/CNTs hybrid material. At 0.5 C, its initial discharge specific capacity is 170 mAh/g, at 3.0 C, its discharge capacity remains at 150 mAh/g. With the rate increase, however, its discharge specific capacity quickly decreases. At 10.0 C, its capacity is 137 mAh/g; at 20.0 C, it is 115 mAh/g; and at 30.0 C, its capacity remains at only about 86 mAh/g. In contrast, the $Li_4Ti_5O_{12}$/G/CNTs hybrid material displays relatively higher discharge specific capacity at different rates. Moreover, the discharge capacities of the $Li_4Ti_5O_{12}$/G/CNTs hybrid material manifest less capacity degradation with the rate increase than that of the pristine $Li_4Ti_5O_{12}$. For example, at 0.5 C, the initial discharge specific capacity of the $Li_4Ti_5O_{12}$/G/CNTs is 174 mAh/g, which is very close to the theoretical value of the spinel $Li_4Ti_5O_{12}$ (175 mAh/g). At 5.0 C and 10.0 C, it is 164 mAh/g and 162 mAh/g; and even at 20.0 C and 30.0 C, it can still remain at 156 mAh/g and 150 mAh/g. These results indicate that the $Li_4Ti_5O_{12}$/G/CNTs hybrid material has higher discharge specific capacity and better rate capability than that of the pristine $Li_4Ti_5O_{12}$. This should be attributed to that the nanosized $Li_4Ti_5O_{12}$/G/CNTs hybrid material has less particle agglomeration and bigger BET surface area, which could reduce the distance for lithium ion diffusion and provide for a higher electrode/electrolyte contact surface area, resulting in the $Li_4Ti_5O_{12}$/G/CNTs hybrid material has faster Li^+ conductivity than that of the pristine $Li_4Ti_5O_{12}$. Moreover, as the CNTs acting like bridges, which could give more effective conductive nets in the electrode of the $Li_4Ti_5O_{12}$/G/CNTs, resulting in the $Li_4Ti_5O_{12}$/G/CNTs hybrid material has better electronic conductivity than that of the pristine $Li_4Ti_5O_{12}$.

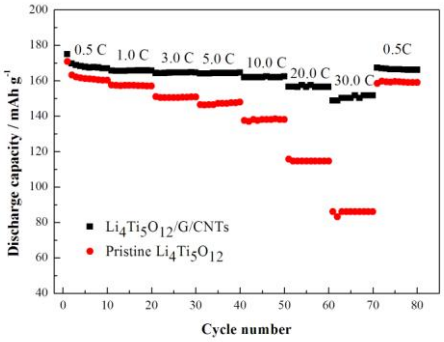

Figure 6. Discharge specific capacity of the pristine $Li_4Ti_5O_{12}$ and the $Li_4Ti_5O_{12}$/G/CNTs hybrid material at different rates.

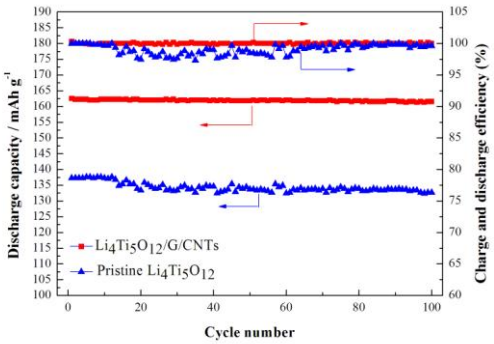

Figure 7. Cyclic performances and charge-discharge efficiencies of the pristine $Li_4Ti_5O_{12}$ and the $Li_4Ti_5O_{12}$/G/CNTs hybrid material at 10.0 C.

For evaluating the cycling stability of the $Li_4Ti_5O_{12}$/G/CNTs hybrid material, it is further charge-discharged at a current rate of 10.0 C for another 100 cycles after the 80 cycles progressive rate tests mentioned in Fig.6. For comparison, the pristine $Li_4Ti_5O_{12}$ sample is also tested under the same conditions. The results are shown in Fig. 7, from which it can be observed that the nanosized $Li_4Ti_5O_{12}$/G/CNTs hybrid material shows a stable cycle life. The initial discharge specific capacity of the $Li_4Ti_5O_{12}$/G/CNTs is 162 mAh/g. After 100 charge-discharge cycles, its discharge capacity remains at 161 mAh/g, and the capacity retention ratio is 99.4%. However, the pristine $Li_4Ti_5O_{12}$ shows a poor cycle life as compared with the $Li_4Ti_5O_{12}$/G/CNTs. Its initial discharge specific capacity is 137 mAh/g. After 100 cycles, its discharge capacity remained at 132 mAh/g, and the capacity retention ratio is 96.3%. Furthermore, as shown in Fig. 7, the charge and discharge efficiency of the $Li_4Ti_5O_{12}$/G/CNTs hybrid material is also better than that of pristine $Li_4Ti_5O_{12}$.

For comparison, the nanosized $Li_4Ti_5O_{12}$/graphene ($Li_4Ti_5O_{12}$/G) hybrid material was also synthesized via a similar sol-gel approach as the $Li_4Ti_5O_{12}$/G/CNTs hybrid material in this paper. The discharge specific capacity of the $Li_4Ti_5O_{12}$/G hybrid material and the $Li_4Ti_5O_{12}$/G/CNTs hybrid material at different rates are shown in Table 2. From table 2, it can be observed that the $Li_4Ti_5O_{12}$/G/CNTs has high discharge capacity than that of the $Li_4Ti_5O_{12}$/G at different rates, which

indicates that the $Li_4Ti_5O_{12}$/G/CNTs has better rate capability than $Li_4Ti_5O_{12}$/G. In addition, the $Li_4Ti_5O_{12}$/G/CNTs hybrid material in the present study also exhibits better rate capability than the $Li_4Ti_5O_{12}$/G hybrid material reported by other authors such as references [24] and [25]. These results indicate that it can obtain better rate capability via synthesizing the $Li_4Ti_5O_{12}$ hybrid material consisting of two conductive second phases (graphene and CNTs).

Table 2. Discharge capacity of the $Li_4Ti_5O_{12}$/G and the $Li_4Ti_5O_{12}$/G/CNTs at different rates.

Materials	0.5 C	1.0 C	3.0 C	5.0 C	10.0 C	20.0 C	30.0 C
$Li_4Ti_5O_{12}$/G (mAh/g)	170	161	158	156	151	138	124
$Li_4Ti_5O_{12}$/G/CNTs (mAh/g)	174	165	164	164	162	156	150

4. CONCLUSIONS

We in situ synthesized the $Li_4Ti_5O_{12}$/G/CNTs hybrid material via a facile sol-gel reaction route. The results indicate that the primary particles of the $Li_4Ti_5O_{12}$ in the hybrid material are nanosized. The $Li_4Ti_5O_{12}$ can anchor or cover on the surface of graphene and CNTs by using the sol-gel method. SEM image also shows that part of the bigger $Li_4Ti_5O_{12}$ particles can not anchor on the surface of graphene. Nevertheless, the CNTs acting like bridges, which can connect the bigger $Li_4Ti_5O_{12}$ particles and the graphene, giving a more effectively conductive connection in the $Li_4Ti_5O_{12}$/G/CNTs hybrid material. Furthermore, the $Li_4Ti_5O_{12}$/G/CNTs hybrid material has less particle agglomeration and bigger BET surface area than that of the pristine $Li_4Ti_5O_{12}$, which indicates that the addition of graphene and CNTs in the precursor can hinder the particle agglomeration and growth during the calcination process. The cyclic voltammograms and AC impedance spectra indicate that the $Li_4Ti_5O_{12}$/G/CNTs has faster Li^+ and better electronic conductivity than that of the pristine $Li_4Ti_5O_{12}$, which should be ascribed to the less particle agglomeration and the more effectively conductive nets existing in the electrode. The nanosized $Li_4Ti_5O_{12}$/G/CNTs hybrid material exhibits excellent rate capability and cycling performance, which is a promising anode material for high-rate lithium ion batteries.

ACKNOWLEDGEMENTS
This work was carried out with financial support from the National Natural Science Foundation of China (No. 51302232), the Ministry of Science and Technology of the People's Republic of China (No. 2011CB932604), the Education Department of Sichuan Province (No. 13ZB0205), and the Innovative Research Team of Southwest Petroleum University (No. 2012XJZT002).

References

1. K. Zaghib, M. Dontigny, P. Perret, A. Guerfi, M. Ramanathan, J. Prakash, A. Mauger, C.M. Julien, *J. Power Sources* 248 (2014) 1050-1057.
2. Izabela Stepniak, *J. Power Sources* 247 (2014) 112-116.

3. M. Kitta, T. Akita, S. Tanaka, M. Kohyama, *J. Power Sources* 237 (2013) 26-32.
4. K.S. Park, A. Benayad, D.J. Kang, S.G. Doo, *J. Am. Chem. Soc*. 130 (2008) 14930–14931.
5. L.F. Shen, C.Z. Yuan, H.J. Luo, X.G. Zhang, K. Xu, F. Zhang, *J. Mater. Chem*. 21 (2011) 761-767.
6. M. Wagemaker, E.R.H. Van Eck, A.P.M. Kentgens, F.M. Mulder, *J. Phys. Chem*. B 113 (2008) pp 224-230.
7. J.S. Park, S.H. Baek, Y.-П. Jeong, B.Y. Noh, J.H. Kim, *J. Power Sources* 244 (2013) 527-531.
8. C.F. Lin, M.O. Lai, L. Lu, H.H. Zhou, Y.L. Xin, *J. Power Sources* 244 (2013) 272-279.
9. Q.Y. Zhang, C.L. Zhang, B. Li, D.D. Jiang, S.F. Kang, X. Li, Y.G. Wang, *Electrochim. Acta* 107 (2013) 139-146.
10. Q.Y. Zhang, C.L. Zhang, B. Li, S.F. Kang, X. Li, Y.G. Wang, *Electrochim. Acta* 98 (2013) 146-152.
11. Y.S. Lin, J.G. Duh, *J. Power Sources* 196 (2011) 10698-10703.
12. C. Lai, Y.Y. Dou, X. Li, X.P. Gao, *J. Power Sources* 195 (2010) 3676-3679.
13. J.Z. Chen, L. Yang, S.H. Fang, S. Hirano, K. Tachibana, *J. Power Sources* 200 (2012) 59-66.
14. Y. Ding, G.R. Li, C.W. Xiao, X.P. Gao, *Electrochim. Acta* 102 (2013) 282-289.
15. G.L. Yang, Z. Su, H.S. Fang, Y.C. Yao, Y.M. Li, B. Yang, W.H. Ma, *Electrochim. Acta* 93 (2013) 158-162.
16. H.G. Jung, N. Venugopal, B. Scrosati, Y.K. Sun, *J. Power Sources* 221 (2013) 266-271.
17. Z.M. Liu, N.Q. Zhang, Z.J. Wang, K.N. Sun, *J. Power Sources* 205 (2012) 479-482.
18. M. Krajewski, M. Michalska, B. Hamankiewicz, D. Ziolkowska, K.P. Korona, J.B. Jasinski, *J. Power Sources* 245 (2014) 764-771.
19. M.E. Stournara, V.B. Shenoy, *J. Power Sources* 196 (2011) 5697-5703.
20. Y. Ding, G.R. Li, C.W. Xiao, X.P. Gao, *Electrochim. Acta* 102 (2013) 282-289.
21. Y. Shi, L. Wen, F. Li, H.M. Cheng, *J. Power Sources* 196 (2011) 8610-8617.
22. X. Li, M.Z. Qu, Y.J. Huai, Z.L. Yu, *Electrochim. Acta* 55 (2010) 2978–2982.
23. Y.B. He, F. Ning, B.H. Li, Q.S. Song, W. Lv, H.D. Du, D.Y. Zhai, F.Y. Su, Q.H. Yang, F.Y. Kang, *J. Power Sources* 202 (2012) 253–261.